Composites Part A 122 (2019) 8–17

Contents lists available at ScienceDirect

Composites Part A

journal homepage: www.elsevier.com/locate/compositesa

Interface properties and their effect on the mechanical performance of flax fibre thermoplastic composites

W. Woigk[a,b], C.A. Fuentes[c], J. Rion[d], D. Hegemann[e], A.W. van Vuure[c], C. Dransfeld[b,f], K. Masania[a,b,*]

[a] Complex Materials, Department of Materials, ETH Zürich, CH-8093 Zurich, Switzerland[1]
[b] Institute of Polymer Engineering, FHNW University of Applied Sciences and Arts Northwestern Switzerland, CH-5210 Windisch, Switzerland
[c] Department of Materials Engineering, KU Leuven, B-3001 Heverlee, Belgium
[d] Bcomp Ltd., CH-1700 Fribourg, Switzerland
[e] Empa, Swiss Federal Laboratories for Materials Science and Technology, CH-9014 St. Gallen, Switzerland
[f] Aerospace Manufacturing Technologies, Faculty of Aerospace Engineering, Delft University of Technology, Kluyverweg 1, 2629 HS Delft, the Netherlands[1]

ARTICLE INFO

Keywords:
A. Natural fibre composites
B. Thermoplastic matrices
C. High toughness
D. Interface

ABSTRACT

Natural fibre (NF) reinforced composites offer high specific mechanical properties and are an ecological alternative to synthetic fibre-reinforced composites. While having great potential, their use today is limited to non-structural applications, mostly with epoxy or polypropylene matrices. This work studies suitable high-performance thermoplastic matrices and characterises their bulk properties, fibre-wetting and composite mechanical behaviour. Thermoplastic polymers such as poly-L-lactide (PLLA) and polyoxymethylene (coPOM) are matrices with bulk properties similar to epoxy. The results show that PLLA matrix NF-composites have a longitudinal modulus and strength of 27 GPa and 308 MPa. The tougher coPOM matrix NF-composites show both high transverse stiffness and strength of 2.6 GPa and 41.5 MPa and show that even the drawback of creep can be overcome by the use of hierarchically structured coPOM. The developed NF-composites demonstrate in-plane properties comparable to those with epoxy matrices and can outperform them by up to 26% in the transverse direction.

1. Introduction

High performance lightweight materials such as those reinforced with E-glass (GF) or carbon fibres (CF) are stiff and strong materials that are widely used in the aerospace, automotive and sports equipment sectors. Despite their excellent mechanical properties, they are highly energy intensive to manufacture with limited recycling at end of use. Composites reinforced by natural fibres (NF) can provide a more sustainable and circular alternative as a structural fibre due to their high specific properties at a lower cost whilst having a low carbon footprint [1–3]. For example, flax fibres have low density [4], Young's modulus up to 80 GPa [2] and capture 1.3–1.4 kg CO_2/kg during their growth, with production emissions of 0.79 kg CO_2/kg fibre [5], thus net CO_2 negative in production. They require 6.5 MJ/kg of energy to extract and produce into continuous structural fibres, being 3.5- and 30-fold lower than GF and CF, respectively [5,6], whilst demonstrating superior specific properties to equivalent GF composites [7–9], albeit still lower than CF composites.

Despite being composed of relatively weak constituents, NFs offer excellent specific tensile [10] and damping [9,11] properties through their hierarchically arranged discontinuous architecture. Their composites allow exploitation of their low material density and high fibre volume fractions, which allows for greater freedom in design [12]. However, their constituents are weak in comparison [13], i.e. about half as strong in tension and compression than glass fibres due to the discontinuous elements and abundance of amorphous biopolymers, holding all the cellulose fibres together. Therefore, in the absence of cell mechanical interlocks [14], the role of the matrix is crucial in enabling stress transfer between the technical fibres, which are a collection of elementary fibres, as well as between fibre tows in the composite material. Typically, high performance NF composites have been produced using epoxy (EP) matrices. They offer high stiffness, low creep and efficient stress transfer between fibres via covalently bonded interfaces to the fibre surface [15,16]. Combined with ease of processing into NF

* Corresponding author at: Complex Materials, Department of Materials, ETH Zürich, CH-8093 Zurich, Switzerland.
E-mail address: kunal.masania@mat.ethz.ch (K. Masania).
[1] Current address.

https://doi.org/10.1016/j.compositesa.2019.04.015
Received 28 November 2018; Received in revised form 12 April 2019; Accepted 13 April 2019
Available online 15 April 2019
1359-835X/

thermoset composites, their composites typically demonstrate low porosity due to the low viscosity of monomer resins [16] and excellent impregnation [17]. However, thermoset-based matrices require careful storage and handling, are highly defect sensitive, brittle and cannot be readily recycled.

As an alternative, thermoplastic matrices offer a more sustainable solution because they allow simple storage and low-cost processing and can lead to materials with intrinsically high toughness. They can be thermoformed and combined with existing injection moulding technologies at high production rates and with low cycle times. Further, end-of-life NF thermoplastic composites can be recycled, making them circular and sustainable materials. Due to the higher melt viscosity of thermoplastic matrices compared to thermosets, processing presents a challenge, and since the fibre matrix adhesion is governed mainly by physical and mechanical interactions for typical thermoplastics, interfacial strength is paramount [16,18]. Until now, their implementation has been mostly limited to matrices such as polypropylene (PP) [19,20] for economic reasons, resulting in intrinsically weaker materials with poor interfaces and high creep, therefore they have been primarily utilised for non-structural applications. Polymers such as polylactic acids (PLA) are attractive bio-based thermoplastic matrices due to their high mechanical performance combined with good processing [2,21], however, they still lack the environmental stability to be used in engineering applications. To enable the fabrication of high-performance composites that are composed of biologically architectured reinforcement, this work compares the wetting and interface behaviour of high-performance thermoplastic matrices that are suitable for engineering applications and studies their NF composites by utilising a simple micromechanics model.

2. Materials & methods

2.1. Flax fibres

The hierarchal structure of the flax fibre (Linum usitatissimum) offers high specific stiffness and strength and outstanding vibration damping behaviour [11]. Extracted from the stem of the flax plant (Fig. 1), the fibres belong to the group of bast fibres. On a macroscopic scale, the outer part of the stem is mainly composed of fibre bundles which comprise several elementary fibres held together by secondary amorphous materials such as pectin, lignin and hemicelluloses [10]. When fibre bundles are used in composites, these are known as technical fibres and their final morphology, length, shape, thickness and number of elementary fibres not only depends on the biological structure of the plant, but also on the extraction process [22]. Technical fibres may exhibit a length of up to 1 m and a diameter between 100 and 200 μm. Elementary fibres are composed of concentrically arranged cell walls, which are about 20–40 mm in length and about 10–40 μm in diameter [23–25]. The second, S2 layer, consists of cellulose microfibrils of crystallised and amorphous cellulose molecules, which interact via hemicellulose chains. These chains are connected by hydrogen bonds to the cellulose microfibril, forming the macrofibril, which is embedded in a matrix of hemicellulose and lignin [26]. The cellulose fibrils have a degree of crystallinity of up to 90% [27] and are helically wound with a micro-fibrillar angle (MFA) of about 10°, giving the fibre its excellent elastic properties [10].

Single technical flax fibres and wet spun UD-woven flax fibre fabrics (ampliTex™ UD type 5009) with an areal weight of 300 g/m^2 were provided by Bcomp Ltd. (Fribourg, Switzerland). The yarns have a nominal linear density of 105 tex and exhibit a twist level of 260 ± 40 turns per metre. Natural fibres are known to have a low decomposition temperature of about 170–190 °C depending on the atmosphere and exposure time to high temperatures [28]. Therefore, the polymers that are used in order to manufacture NF-reinforced composites must allow for processing below the fibre's degradation temperature as discussed in the next section.

2.2. Matrix polymers

Polymers may be classified by the resource basis of the material and by their compatibility with the environment. In other words, classes of polymers can be divided into four main groups; fossil-based or bio-based and non-biodegradable or biodegradable. Materials often referred to as bio-plastics are bio-based or biodegradable or even both. In this study, polypropylene (PP) and epoxy resin (EP), both non-biodegradable and fully fossil-based [29], serve as benchmark materials due to their wide spread use in industrial applications. PP is a very low cost, low-density, semi-crystalline thermoplastic polymer with moderate quasi-static mechanical properties and low environmental impact [30]. The PP 515A type, supplied by Sabic, was used in this study. According to the manufacturer's data sheet, this PP has a melt flow index (MFI) of 24 g/10 min at 230 °C and 2.16 kg weight [31].

EP in contrast is a group of thermoset polymers which offer good mechanical properties, which may be processed at room temperature due to their low viscosities. However, the epoxy resources are ecologically unfriendly and their recycling highly limited. In this study, a diglycidyl ether of bisphenol A (DGEBA) epoxy resin, Araldite XB 3585, in combination with a diethylenetriamine and 4,4′-*iso*-

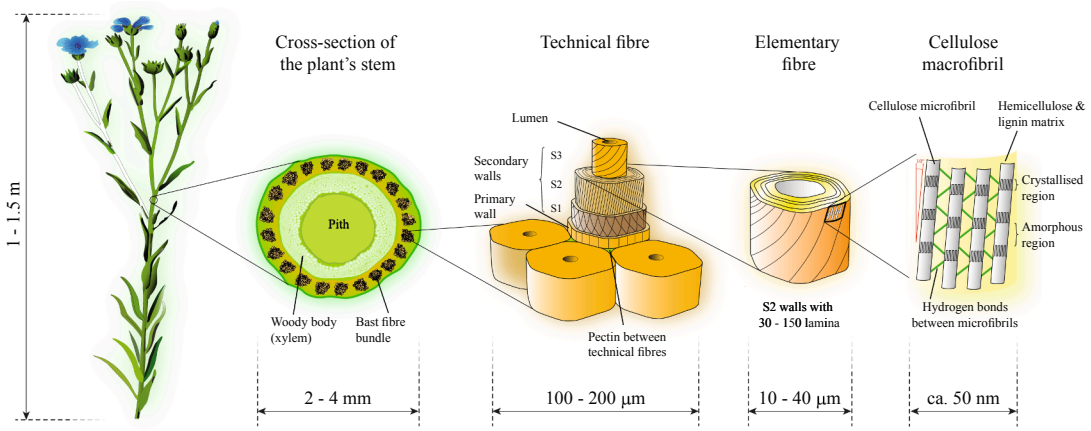

Fig. 1. Multi-scale hierarchical structure of flax fibres. The elongated fibres are situated in the stem's sclerenchyma, in which the bast fibre occur in bundles. The technical fibres consist of several elementary fibres which are held together by pectin. An elementary fibre is composed of concentrically arranged cell walls. The S2 layers in the secondary cell walls are assembled out of several lamina of highly aligned cellulose microfibrils embedded in a hemicellulose (20 wt%) and lignin (2 wt %) matrix which are connected through hydrogen bonds.

propylidenediphenol mixture hardener, Aradur XB 3458, both supplied by Huntsman Advanced Materials (Basel, Switzerland) were used. A resin-to-hardener weight ratio of 100:19 was used. This formulation typically yields a glass transition temperature of 100–110 °C with the recommended cure cycles.

Polylactic acids (PLAs), belong to a group of polymers which are both bio-based and biodegradable. PLAs are thermoplastic polymers whose isomers are usually derived from sugarcane or corn. PLAs can be amorphous, but also semi- and highly crystalline with high mechanical properties. Those properties, however, come with the cost of very low fracture toughness and brittle failure. Here, the L100H PLLA, an L-lactic acid isomer type of PLA, supplied by Sulzer Chemtech Ltd (Winterthur, Switzerland), with an MFI of 6–7 g/10 min at 190 °C and 2.16 kg was used. The melting temperature of the PLLA is reported as 180 °C [32].

Polyoxymethylene as a copolymer (coPOM) of formaldehyde (CH_2O) and ethylene oxide (C_2H_4O) is another engineering plastic which is already extensively used in automotive industries because of its high mechanical properties and excellent dimensional stability. The very high degree of crystallinity, the low creep and the comparatively low melt temperature make coPOM a very suitable polymer as matrix material for NF composites. As coPOM, the Hostaform C 9021 XAP copolymer (Celanese, USA), with an MFI of 11 g/10 min at 190 °C and 2.16 kg was used. To further enhance the mechanical performance through a hierarchical reinforcement at a finer length scale, a 10 wt% glass fibre filled coPOM (coPOM_GV10), Hostaform C 9021 GV1/10 (Celanese, USA) with an MFI of 9 g/10 min at 190 °C and 2.16 kg was also considered. The melting temperature of both coPOM materials is reported as 166 °C [33,34].

2.3. Rheological measurements

The complex viscosity of polymer was measured according to ISO 11443 using a Physica MCR 300 (Anton Paar, Buchs, Switzerland). The polymers were heated to 190 °C and measured using a plate-plate method (25 mm diameter plate) at frequencies between 100 and 0.1 Hz using a gap of 1.6 mm to avoid slippage at the plate polymer interface.

2.4. Charpy impact measurements

Charpy impact tests were conducted on a Zwick 5102 Charpy impact testing machine (Zwick GmbH & Co. KG, Ulm, Germany). A pendulum of capacity 7.5 J was used for the bulk polymer impact testing. Frictional effects were removed by a specimen-free calibration. In the notched samples, a machined v-shaped notch was cut via drawing of a sharp blade followed by tapping.

2.5. Contact angle measurement and surface energy analysis

Advancing and receding contact angles of various test liquids of analytical grade (ultrapure water: 18.2 Ω cm resistivity, diiodomethane ≥ 99%: Acros, and ethylene glycol ≥ 99%: Sigma–Aldrich) were measured on the polymer films and flax technical fibres at room temperature (20 °C) and relative humidity of 50% on a Krüss K100 SF tensiometer using the Wilhelmy technique [16,35]. The technique consists of measuring the forces exerted by a liquid on a solid substrate with known perimeter while the substrate is immersed or removed from a test liquid [35]. A microbalance measures a force ($F_{measured}$), which is the sum of the capillary force ($F_{wetting}$), the weight of the fibre (G) minus the buoyancy force ($F_{buoyancy}$):

$$F_{measured} = F_{wetting} + G - F_{buoyancy} \quad (1)$$

When the weight of the probe is known and accounted for, only the wetting and buoyancy forces remain which can be expressed as:

$$F_{measured} = p\gamma\cos\theta - \rho g A d \quad (2)$$

where p is the fibre perimeter, γ the liquid surface tension, θ the contact angle of the liquid on the fibre, ρ the liquid density, d the immersion depth, and $A$the fibre cross-sectional area (here taken constant and assuming the fibre to be a perfect circular cylinder).

The average of the cosines of the dynamic advancing (θ_{adv}) and dynamic receding (θ_{rec}) angles at a contact-line velocity of 1.5 mm/min were used to estimate the cosine of the equilibrium angle (θ_{equ}) so that both the low and the high surface energy components of the analysed surfaces could be considered in the analysis [36]. Due to surface irregularities [35], receding angles were not possible to measure for flax technical fibres, therefore, only advancing angles were used.

The method applied to determine the fibre perimeter was by using its density, mass and length to determine the apparent perimeter [16,35]. When hexane (0° contact angle) is used and the force is extrapolated back to zero immersion depth, Eq. (2) simplifies to:

$$F = p\gamma \quad (3)$$

where F is the measured wetting force. At relatively low speeds, very low surface tension hexane was assumed to have a contact angle of 0° with all substrates [35]. Three test liquids were selected to show a low condition number value corresponding to a good combination of dispersive, acidic and basic liquids, which reduces the influence of the number and choice of liquids [37]. Surface energy components were calculated according to the Van Oss model and by using the SurfTen 4.3 software [38]. The work of adhesion (W_a), and the interfacial energy (γ_{sl}) could subsequently be calculated according to the following equations:

$$W_a = \gamma_s + \gamma_l - \gamma_{sl} \quad (4)$$

$$\gamma_{sl} = (\sqrt{\gamma_s^{LW}} - \sqrt{\gamma_l^{LW}})^2 + 2(\sqrt{\gamma_s^{+}} - \sqrt{\gamma_l^{+}})(\sqrt{\gamma_S^{-}} - \sqrt{\gamma_l^{-}}) \quad (5)$$

where $\gamma_{s,l}$ represents the surface energy (solid and liquid respectively), $\gamma_{s,l}^{LW}$ represents the Lifshitz-van der Waals component,$\gamma_{s,l}^{+}$ represents the acidic, and $\gamma_{s,l}^{-}$ the basic component.

2.6. Thermoplastic film production

Films with a width of 80 mm and a thickness of approximately 100 μm were produced using a Collin (Dr. Collin GmbH, Germany) Teach-Line extruder equipped with a slit die. The feedstock materials, in the form of pellets, were dried overnight and fed to the extrusion machine. The temperatures of the heating zones were gradually increased from 50 °C in the feeding zone up to 200 °C for PP and 210 °C for PLLA, coPOM and coPOM_GV10. Films were drawn from the extruder die through two rotating and water-cooled rollers and collected to a winding cylinder.

2.7. Composite processing

The NF thermoplastic composites were manufactured via film stacking using pre-dried fabrics (vacuum oven at 110 °C at 20 kPa for 15 min) and pre-dried polymer films which were stacked alternately with flax fibres in a steel mould. The orientation of the foils was maintained such that the extrusion direction remained parallel to the fibre direction. A reference fibre volume content of 50 vol% was used in order to calculate the number of alternating layers required for flax fabric and polymer film to provide fair comparison with the NF thermoset composite. Six unidirectional (UD) flax layers were stacked to press composites with a nominal thickness of 2 mm. The mould was placed in a 190 °C pre-heated press (Vogt P200T-2E, Germany) and a piston pressure was applied resulting in a cavity pressure of 1 MPa. After 10 min pressing at 190 °C, the mould was transferred to the cooling level of the press and pressure was re-applied and maintained during the cooling cycle.

EP matrix NF composites were prepared similarly using six layers of flax fibres placed in the mould using a compression resin transfer moulding process [39,40] and cured at 80 °C for 20 min followed by

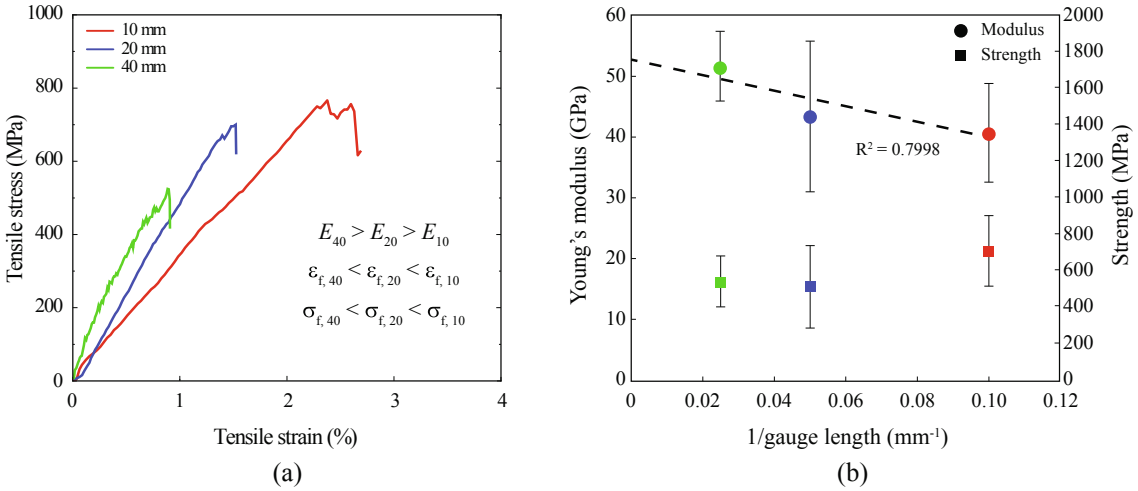

Fig. 2. Tensile properties of technical flax fibres: (a) Stress-strain diagram of representative curves of the investigated gauge lengths (b) Young's modulus and tensile strength of flax technical fibres as a function of 1/gauge length.

post-curing at 100 °C for 20 min. The amount of matrix was calculated to achieve a composite with a fibre volume content of about 50%.

2.8. Microscopy and image analysis

Samples for microscopy and image analysis were prepared by cutting composites in the longitudinal direction, placing them in cylindrical potting container and afterwards filling these containers with polyurethane potting resin (CEM9000, Cloeren Technology GmbH, Germany). After resin curing, the bottom surfaces of the samples were polished using a Struers LaboPol-25 (Struers GmbH, Germany) grinding machine, gradually reducing the grain size of the grinding paper down to 5 µm. The images were taking with a laser confocal microscope, VK-9710 (Keyence, Germany). The image analysis was conducted using the ImageJ software package with its ability to run user-defined macros. The macro used modified the pristine images in such a way that fibres, matrix and voids could be clearly distinguished and the area distribution measured.

2.9. Tensile testing

2.9.1. Technical fibre

Technical flax fibres were tested at three different gauge lengths (10, 20, and 40 mm) using a mini-Instron 5942 equipped with a 100 N load cell at 20 °C and 50% RH. The crosshead speed was 1.0 mm/min. For each gauge length, ten randomly selected technical fibres were inspected using a microscope to verify the absence of major damage, and then conditioned at 20 °C and 50% RH for more than one week. The density of technical fibres of flax (1.44 g/cm^3) was determined using a gas pycnometer. Each individual technical fibre was then weighed and the cross-sectional area calculated using its density, mass and length, assuming that the technical fibre has a constant cross-section. The strain was calculated as the ratio of the change in the clamping length, recorded by the crosshead displacement, to the initial clamping length. To account for the compliance of the testing machine together with the tensile setup, a compliance calibration using a steel bar was carried out and the displacement subtracted from the individual test results.

2.9.2. Polymers

Tensile tests were carried out on injection moulded polymer dog bone shaped specimens (DIN EN ISO 527-1). The tests were conducted at a displacement-controlled rate of 50 mm/min using a universal testing machine (walter + bai ag, Switzerland) equipped with a 100 kN capacity load cell. The deformation was measured using a clip-on extensometer with an initial gauge length, l_0, of 50 mm. The Young's modulus was determined as the secant modulus between 0.05 and 0.25% strain.

2.10. Flexural testing

Flexural composite properties were determined using three-point bending measurements in accordance with ISO 14125. Tests were conducted for NF composites with longitudinal (0°) and transverse (90°) fibre orientation. A span of 40 mm between the two supports was chosen in order to allow for a span-to-thickness ratio greater than 16. Flexural tests were conducted on a universal testing machine (walter + bai ag, Switzerland), equipped with a 1 kN capacity load cell. The flexural deflection was measured with an external linear variable differential transformer (LVDT) that recorded precisely the flexural deformation of the specimen's lower surface (tensile side). To account for potential variations in the fibre volume fraction as a result of the manufacturing of the different polymer composites, the longitudinal flexural properties were linearly normalised to a fibre volume fraction of 50%.

3. Results

3.1. Technical fibre tensile properties

The tensile properties of fibres are a key parameter for the design of composites and allows use of micro-mechanical models to describe properties analytically. The performance of technical flax fibres in tension were measured using three different clamping lengths, which allows to exclude potential effects of slippage and testing machine compliance on the mechanical properties. The Young's moduli and strengths for the three different gauge length of technical fibres were recorded according to Defoirdt et al. [41]. Fig. 2(a) shows representative stress-strain curves for each of the investigated gauge lengths considered. With increasing gauge length, the Young's modulus, E_i, increases, whereas the strain to failure, $\varepsilon_{f,i}$, and the strength, $\sigma_{f,i}$, show an opposite relationship. Fig. 2(b) shows the Young's modulus as a function of the inverse of the gauge length with an increasing value for Young's modulus for decreasing gauge length. At infinite fibre length, the displacement that is not caused by the elongation of the fibre, i.e. slippage and machine compliance, can be excluded. As clearly shown in Fig. 2(b), the measured moduli depend on the test length, suggesting an influence of slippage. Thus, by linear extrapolation, the fibre modulus at infinite fibre length could be estimated to be about

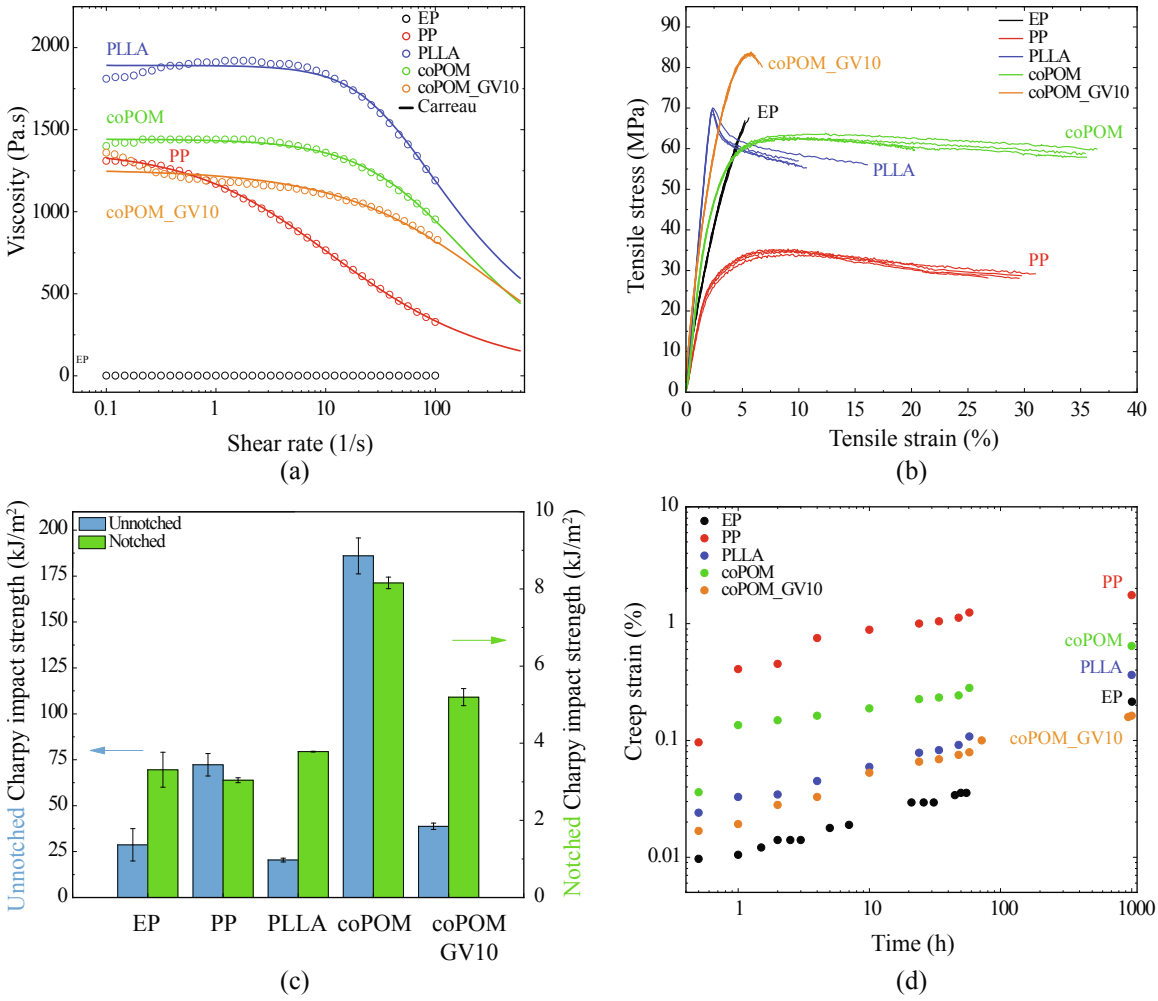

Fig. 3. Bulk polymer mechanical properties: (a) Melt viscosity as a function of the angular shear frequency with measurements fit to the Carreau model, (b) Tensile stress-strain behaviour, (c) Charpy impact strength of unnotched (left axis) and notched specimens (right axis) and (d) Three-point bending creep-strain time diagram.

52.6 GPa.

The mean tensile strength and standard deviations employing a normal distribution as a function of gauge length of the flax technical fibres are also shown in Fig. 2(b). The strength shows the tendency to decrease as the gauge length increases, since the longer the fibre, the higher the likelihood of defects in the architecture where the fibre can break prematurely [42]. Due to the large scatter, the strength was calculated as the mean value of all tested fibres without making distinction of the gauge length, obtaining the value of 590.6 ± 130.4 MPa.

3.2. Polymer matrix properties

The polymer melt viscosity was measured as a function of a sinusoidal applied shear strain in a parallel plate rheometer configuration in order to better understand the material behaviour of the polymer in the liquid state. The measured viscosities as a function of the rotational frequency are shown in Fig. 3(a). The thermoplastic polymers initially exhibit melt viscosities that are independent from the applied shear rate, as indicated by the plateau in the viscosity vs shear-rate curve. However, this was only valid in the small range away from the zero-shear rate, η_0. At higher shear rates, the expected shear thinning behaviour became apparent. In order to better understand and to describe the rheological behaviour of the polymers, the Carreau model (Eq. (6)) can be fit to the measured values (see solid lines in Fig. 3(a)).

$$\eta(\dot{\gamma}) = \eta_\infty + (\eta_0 - \eta_\infty)[1 + (\lambda\dot{\gamma})^a]^{\frac{(n-1)}{a}} \quad (6)$$

where η_0 and η_∞ are the plateau viscosities for zero-shear rate and infinite-shear rate, respectively, λ the natural time, a determines the transition from Newtonian plateau to power-law region and n is the power-law index, whereas $n - 1$ is the slope. With this model, one can determine the critical shear rate, $1/\lambda_c$, i.e. when the term $\lambda_c\dot{\gamma}$ equals unity. The critical shear rate indicates the shear rate at which the viscosity decreases, thus describing the transition from Newtonian to power-law behaviour [43]. The model also describes the flow behaviour beyond the measurable frequency range. The five parameters that were determined via least squares method to result in the best fit to the experimental data points are provided in Table 1.

An estimate for the shear rate regime in the compression moulding processing can be derived assuming a linear viscosity gradient between two fibre bundles, where the flow velocity at the fibre's surface is taken

Table 1
Carreau model characteristic values and fitting parameters.

Material	η_0 (Pa s)	η_∞ (Pa.s)	λ (s)	n (–)	a (–)
PP	1257	0	0.00122	0	0.6
PLLA	1892	1	0.02585	0.6	1.5
coPOM	1442	0	0.00945	0.37704	1
coPOM_GV10	1257	0	0.00122	0	0.6

Table 2
Shear rate estimation for NF impregnation.

Material	η_0 (Pa s)	t_{Darcy} (s)	$\dot{\gamma}\|_{x=0.1mm}$ (s^{-1})	$\dot{\gamma}\|_{x=0.25mm}$ (s^{-1})
EP	0.5	0.004	1557	623
PP	1310	10	0.6	0.24
PLLA	1810	14	0.4	0.17
coPOM	1400	11	0.6	0.22
coPOM_GV10	1410	11	0.6	0.22

to be zero. By using half the distance between two fibre bundles as shearing height and a calculated impregnation time assuming Darcy flow [44], one can obtain the simple relation

$$\dot{\gamma} = \frac{(v_1 - v_0)}{h} = \frac{r_{bundle}/t_{Darcy}}{x/2} = \frac{2 \cdot r_{bundle}}{x \cdot t_{Darcy}} \quad (7)$$

where r_{bundle} is the fibre bundle radius used as vertical flow distance, t_{Darcy} the calculated time to impregnate half of a fibre bundle and x the distance between two fibre bundles. Table 2 lists the results for the estimated shear rates determined using Eq. (7) considering a bundle radius of 0.15 mm and a maximum and minimum distance of 0.25 and 0.1 mm, respectively. The maximum value describes half the distance between the centre points of two adjacent bundles.

The results show and the equation already implies that the shear rate increases with decreasing viscosity as a result of the higher velocity gradient. This holds true at constant impregnation pressure which affects the impregnation time calculated by the Darcy law. The calculated shear rates during film stacking compression moulding are comparatively low, which implies that the melt viscosities during processing are high. Based on these shear rate results, it is assumed that the polymers during the processing have the viscosity at nearly zero shear rate, η_0, determined via rheology measurements (see Fig. 3(a)).

The role of the matrix is to embed the reinforcing fibres and to transfer inter- and intralaminar stresses between adjacent fibres and layers. Since the transverse properties are highly dependent on the matrix and interface properties, we measured the quasi-static tensile properties, Charpy unnotched and notched impact strength and the long-term creep behaviour of the pure polymers. Fig. 3(b) shows the stress-strain curves of the injection moulded bulk polymers tested under uniaxial tension. As a highly cross-linked polymer, the EP measured modulus and strength values of 3.6 GPa and 68 MPa respectively, and failed in a brittle manner with negligible plastic deformation before rupture. The PP measured 1.7 GPa and 35 MPa, respectively and showed a significant plasticity before reaching the maximum stress. In addition, the failure did not occur suddenly but gradually with progressive load shedding and necking of the polymer. The coPOM and the PLLA measured stiffness values in mean of 2.7 GPa and 3.5 GPa, respectively. The short glass fibre reinforced coPOM_GV10 showed a Young's modulus of 3.3 GPa which is very close to the modulus measured for the EP (3.6 GPa), demonstrating a credible thermoplastic equivalent material to EP in terms of stiffness with the PLLA polymer. Regarding the strength of the polymers, one can see that coPOM, PLLA and EP, with 63 MPa, 69 MPa and 68 MPa, respectively, have very similar strengths. However, the curves also reveal that the coPOM specimens did not fracture after the materials' strength was exceeded. Instead, the coPOM specimens exhibited a high strain to failure as compared to EP, PLLA and the coPOM_GV10 specimens. This effect suggests the ability of the coPOM material to dissipate large amount of energy by plastic deformation before failure.

The tensile properties of the injection moulded samples were compared to film stack foils from extrusion in order to characterise the effect of orientation and high shear rate during injection moulding. Young's moduli of 1.6, 3.1, 2.3 and 3.1 GPa were measured for PP, PLLA, coPOM and coPOM_GV10, respectively. The strength values of the film-stacked samples were found to be 37, 61, 58 and 76 MPa for PP, PLLA, coPOM and coPOM_GV10 specimens, therefore the values obtained were very similar to those of the injection moulded samples. The injection moulded sample values were later used for micro-mechanical modelling to avoid influences of surface effects on the measured yield behaviour and strength.

The ability of the matrix to deform plastically is one of the key elements that could contribute to an increased toughness of the fibre reinforced composite [45]. Fig. 3(c) compares the Charpy impact performance of the polymers, showing the dissipated energy values for unnotched and notched specimens as an expression for the materials' toughness. Thermoplastic polymers exhibit generally a much higher toughness as compared to highly cross-linked thermoset polymers. When comparing the benchmark materials, EP and PP, the difference becomes obvious. The unnotched impact strength values for EP and PP are 29 kJ/m^2 and 72 kJ/m^2, respectively. PLLA and coPOM_GV10 measured 20.4 kJ/m^2 and 39 kJ/m^2. The Charpy impact performance of the pure coPOM materials with a Charpy energy of 186 kJ/m^2 is 2.5 times higher than for PP. The notched strength was also evaluated for the polymer matrices in order to describe the defect sensitivity. EP, PP and PLLA were found to measure similar strengths of 3.3 kJ/m^2, 3 kJ/m^2 and 3.8 kJ/m^2, respectively, while CoPOM and coPOM_GV10 reached notched Charpy strength values of 8.15 kJ/m^2 and 5.2 kJ/m^2, respectively. Fig. 3(d) shows the creep properties measured with a flexural three-point bending setup where the specimens' deflections were recorded over time. The PP and the coPOM material show a similar creep behaviour, which can be identified by the rather high instantaneous strain, the high deformation within the first hour of the tests and the progressive strain development. Contrary, PLLA, coPOM_GV10 and EP exhibit a nearly linear progression in the double logarithmic plot. It is interesting to point out that the coPOM_GV10, despite being a thermoplastic polymer, exhibits a lower deflection after 1000 h of loading than the EP.

3.3. Surface energy analysis

Table 3 shows the average of the measured advancing and receding contact angles, and the calculated equilibrium angles for the polymer films, as well as the advancing angles for flax fibres. In Table 4, the surface energy components of the thermoplastic surfaces and flax fibre, calculated using the angles shown in Table 3, are presented. The PP polar surface energy components theoretically should be zero, since pure PP is a non-polar polymer. However, the effect of aging processes, as well as contamination and oxidation, produce a deviation; while not zero, PP did exhibit the lowest polar surface energy components (Lewis base, γ^-, and Lewis acid, γ^+) [46]. On the contrary, both PLLA and

Table 3
Advancing, receding and equilibrium contact angles of probe liquids on flax and thermoplastic surfaces: water (WT), ethylene glycol (EG), diiodomethane (DM).

Liquid	WT			DM			EG		
	adv	rec	equ	adv	rec	equ	adv	rec	equ
Flax fibre	52.6 ± 4.4	–	–	60.2 ± 4.3	–	–	45.0 ± 5.6	–	–
PP	98.2 ± 0.9	78.1 ± 1.1	88.2 ± 1.0	69.5 ± 0.9	45.6 ± 1.2	58.3 ± 1.0	73.3 ± 0.2	54.6 ± 0.3	64.3 ± 0.2
PLLA	85.0 ± 0.8	62.5 ± 0.9	74.1 ± 0.8	60.1 ± 1.9	37.2 ± 1.7	49.6 ± 1.8	58.0 ± 1.1	36.9 ± 0.9	48.3 ± 1.0
coPOM	86.1 ± 0.5	57.4 ± 0.4	72.3 ± 0.4	54.3 ± 1.4	31.4 ± 1.9	44.1 ± 1.5	65.2 ± 0.8	41.0 ± 1.0	54.1 ± 0.9

Table 4
Surface energy components, spreading coefficient, S, and work of adhesion, W_a, of flax fibres and thermoplastic films.

Material	γ^{LW} (mJ/m^2)	γ^- (mJ/m^2)	γ^+ (mJ/m^2)	γ^{tot} (mJ/m^2)	S (mJ/m^2)	W_a (mJ/m^2)
Flax fibre	28.5 ± 1.5	16.7 ± 1.5	0.67 ± 0.47	35.2 ± 2.1	–	–
PP	29.5 ± 0.6	1.7 ± 0.3	0.04 ± 0.02	30.1 ± 0.6	1.59 ± 2.3	61.8 ± 2.3
PLLA	34.5 ± 1.0	4.4 ± 0.4	0.27 ± 0.08	36.7 ± 1.1	−2.97 ± 2.7	70.4 ± 2.7
coPOM	37.5 ± 0.8	5.3 ± 0.2	0.001 ± 0.0	37.6 ± 0.9	−5.77 ± 2.6	69.3 ± 2.6

coPOM have a higher total surface energy due to the presence of the functional groups bonded to their structure (−OH/−CH_3 and −O−CH_3, for PLLA and coPOM respectively), which increases the acid-base polar components and results in polymers also showing higher Lifshitz-Van Der Waals (γ^{LW}) components. Note that the same surface energy was assumed for the coPOM_GV10 as for the coPOM, since the glass fibres in the matrix are not surface active.

The surface composition of flax fibres is more complex. The relative surface atomic fractions and decomposition of C1s peaks obtained by XPS (X-ray photoelectron spectroscopy) for flax fibres used in composites have been recently reported in literature [24], showing 71.2%, 21.5%, 5.6%, and 1.6% for C1, C2, C3, and C4 components respectively, relative to the total C1s peak. The different contributions of functional groups to the shape of the C1s peak have been described in the literature for lignocellulosic materials [16,47–49]; C−(C,H) linkages of lignin and extractives (C1); CC−OH groups of cellulose, hemicelluloses, lignin and extractives, as well as CC−OC−C linkages of lignin and extractives (C2); C═O groups in lignin and extractives, as well as OC−CC−O linkages in cellulose and hemicelluloses (C3); COOH groups of hemicelluloses, as well as COOC and COOH groups of extractives (C4).

According to the literature [47,50–52], these four different components of the carbon peak are related to the physical interactions of materials: C1 may be recognized as representative of aliphatic or aromatic carbon participating in Lifshitz-Van Der Waals interactions; while C2, C3, and C4 might represent polar interactions. The presence of C2, C3, and C4 components up to 30% of the total C1s peak components agrees with the rather polar character of flax fibres deduced from the surface energy components when compared to the thermoplastic films (see Table 4). The high level of C1 component reveals the presence of a notably large number of groups on the flax fibre surface participating in Lifshitz-Van Der Waals interactions, also in agreement with our surface energy estimations (see Table 4).

3.4. Composite flexural properties

To characterise the role of the matrix and the interface on the flexural performance, three-point bending tests on specimens with longitudinal and transverse fibre directions were conducted. The measured flexural moduli (blue bars) and strength values (green bars) are shown in Fig. 4(a) and (b) for longitudinal and transverse directions, respectively. In the longitudinal direction, the EP matrix NF-composites measured an average flexural stiffness of 27 GPa, which represents the highest mean value amongst the matrix materials that were studied. NF-composites with the PP matrix measured the lowest moduli with an average value of 22.1 GPa. The PLLA matrix NF-composites have the same stiffness as the EP NF-composites, with a measured flexural modulus of 27 GPa. Moduli of 23.3 and 23.5 GPa were measured for the coPOM and coPOM_GV10 matrix NF-composites, respectively, showing almost no effect of the short glass fibre in the coPOM_GV10 matrix to the longitudinal composite properties as would be expected. When considering the standard deviation of these two coPOM stiffness values, no difference between the stiffnesses of coPOM and PP matrix NF-composites was observed. Despite a difference in modulus of 20% between the EP and PP matrix NF-composites, the flexural stiffness seems to be less compromised by the matrix materia; as expected the stiffness is governed by the reinforcing fibres. However, the ability to transfer stresses between fibres via the matrix and the fibre/matrix interface and thus also the quality of the impregnation and interface strength becomes particularly important when the composite is exposed to higher strains. This influence can be seen when analysing the ultimate flexural strength. Similar to the stiffness, the EP and PP matrix NF-composites show the highest and lowest values with 337 MPa and 150 MPa, respectively. The PLLA matrix NF-composite strength was measured as 308 MPa. The coPOM matrix NF-composites have an average flexural strength of 228 MPa. Interestingly, the short glass fibre-reinforced coPOM_GV10 matrix NF-composites have a strength of 260 MPa, 14% higher compared to the neat coPOM composites. This gain in strength shows clearly, a contribution of the short glass fibres to the composite's load bearing ability in the longitudinal fibre direction.

Because of the high anisotropy of natural fibres, the fibre properties transverse to the fibre axis are usually a factor 5 to 11 lower [53–55], which increases the importance of the matrix and interface properties. Fig. 4(b) shows the transverse moduli and strengths for the NF-composites. A modulus of 3.4 GPa was measured for the EP matrix NF-composites. The PP matrix NF-composites measured a stiffness of 1 GPa. The PLLA matrix NF-composites reached a modulus of 3.2 GPa, which is very close to the measurement of the neat polymer (3.5 GPa). The coPOM and coPOM_GV10 matrix NF-composites exhibited moduli very similar to the EP matrix NF-composites, i.e. 2.6 and 2.9 GPa, respectively. A similar trend could be observed for the transverse flexural strength. A strength value of 39.3 MPa was measured for EP matrix NF-composites. The coPOM matrix NF-composites with 41.5 MPa and, slightly higher coPOM_GV10 matrix NF-composites with 49.5 MPa, which demonstrates an increase of 6 and 26%, respectively, compared to EP matrix NF-composites. In contrast, the PP and PLLA matrix NF-composites exhibited lower values of 17.8 and 22.5 MPa, respectively. The low strength of PP was believed to be responsible for the low strength of the composite in transverse direction, whereas the brittle behaviour associated with a stress concentration at the fibre matrix/interface is believed to have caused a rather early failure of the PLLA matrix NF-composites.

4. Discussion

To analyse the efficiency of composite properties among the matrices used in this study, the measured properties were compared by a simple longitudinal rule of mixture (RoM) micromechanical model, which considers an efficiency factor (Eq. (8)). This factor represents the percentage of the measured property as compared to the theoretical maximum to quantitatively describe impregnation and interface efficiency. The composite modulus in the longitudinal fibre direction, E, can be calculated as

$$E = k[V_f \cdot E_f + (1 - V_f) \cdot E_m] \tag{8}$$

where k the efficiency factor, V_f the fibre volume fraction, E_f and E_m the fibre and matrix modulus, respectively. E_f was set to 52.6 GPa as measured for the technical fibres (see Section 3.1), whereas the E_m was chosen in accordance with the bulk modulus.

The analysis and calculation of the efficiency factor can be done at $V_f = 0.5$ as the measured moduli were already normalised to a fibre volume fraction of 50%. Table 5 shows the measured and calculated

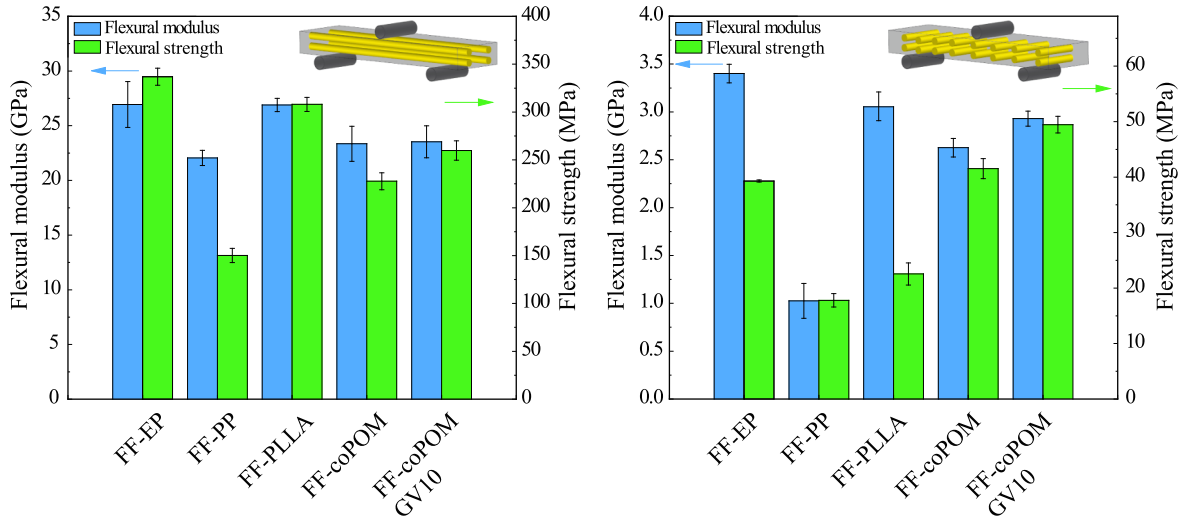

Fig. 4. Flexural properties of unidirectional flax fibre reinforced composites: Modulus (blue bars) and strength (green bars) of specimens tested in (a) longitudinal and (b) transverse direction.

Table 5
Measured and calculated longitudinal flexural composite moduli and stiffness efficiency factor.

Material	$E_{1,measured}$ (GPa)	$E_{1,RoM,k=1}$ (GPa)	k (%)
FF-EP	26.9	27.96	96
FF-PP	22.1	27.13	81
FF-PLLA	26.9	28.07	95
FF-coPOM	23.4	27.66	85
FF-coPOM_GV10	23.6	27.94	84

moduli along with the corresponding efficiency factors. The results show that the PLLA impregnation offers similar performance to that of the EP matrix composites. Due to more difficult impregnation and weaker surface interaction of the polymer, the PP and coPOM matrix NF-composites offer similar magnitudes of k of around 80–85% efficiency.

Fig. 5 shows the NF-composite strengths dependent on the W_a. Mechanical properties were obtained via flexural three-point bending tests in (a) longitudinal and (b) transverse fibre direction. The surface energy analysis (Table 4) suggests that the thermoplastics with negative spreading coefficients will not spontaneously spread on the fibres. Nevertheless, a suitable processing technique that allows for a good fibre impregnation in combination with the constituents will govern the composite mechanical behaviour.

In order to evaluate impregnation quality, the composite morphology was studied through cross-sectional image analysis. Microscopy shows that the impregnation resulted in consistent fibre volume fractions and relatively low porosity in the NF-composites. A representative cross-section of a NF-composite is shown in the inset in Fig. 5(a) and the fibre volume fraction and porosity data listed in Table 6. Therefore, the properties are likely to be governed by the W_a. The correlation for the longitudinal properties shows a tendency of increasing properties with increasing W_a. Longitudinal strength is dominated by the fibre strength associated with the quality of the fibre/matrix interface capable to transfer stresses via shear. Since the W_a for PLLA was measured to be the highest, the strength was found to be superior as compared to the rest of the thermoplastic NF-composites. On the other hand, the W_a for PP was measured to be rather low, resulting in a low failure strength due to the poor interaction at the fibre/matrix interface. Between these two extreme values, the coPOM and coPOM_GV10 NF composites show an intermediate W_a value and thus a slightly lower strength compared to the PLLA matrix NF-composites.

To assess the positive influence of work of adhesion on the transverse strength, the two can be compared. The PP, coPOM and coPOM_GV10 matrix NF-composites show positive correlations,

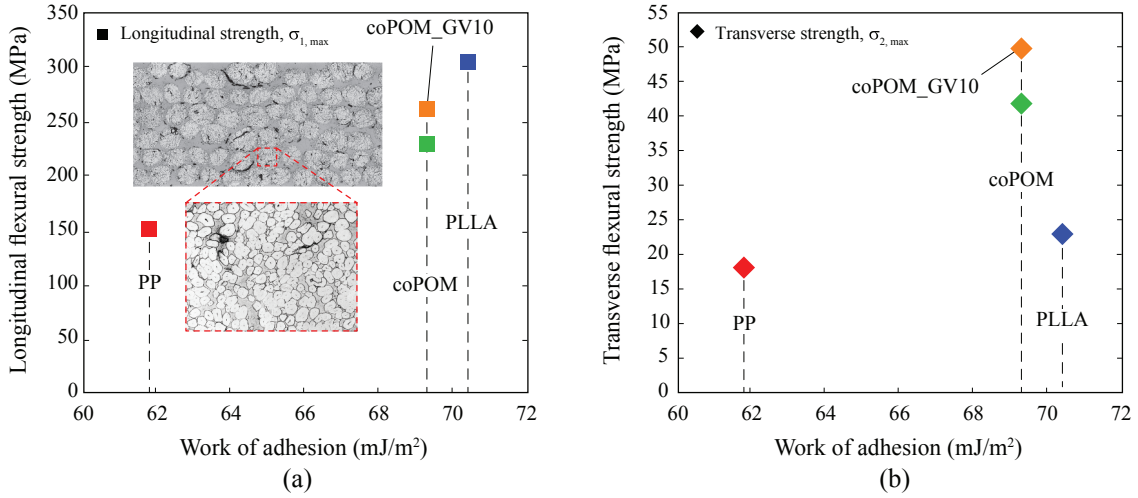

Fig. 5. Flexural strength dependent on the work of adhesion. Properties in (a) longitudinal and (b) transverse direction.

Table 6
Fibre volume fraction and void content of the FF-reinforced composites.

Material	Fibre volume fraction (%)	Void content (%)
FF-Epoxy	48 ± 1	n/a
FF-PP	52 ± 1	1.7 ± 0.2
FF-PLLA	55 ± 2	1.8 ± 0.7
FF-coPOM	48 ± 4	1.4 ± 0.9
FF-coPOM_GV10	50 ± 2	1.2 ± 0.4

however, this is not the case for the PLLA matrix NF-composites. They show a significantly reduced strength despite having the highest W_a amongst the materials tested. This effect might be because of the brittle material behaviour of PLLA when exposed to high strains, as can be seen in the polymer's stress-strain curve in Fig. 3(b). Another explanation could be that the PLLA is not able to completely penetrate in between the technical fibres due to the rather low spreading coefficient (see Table 4). In a poorly impregnated composite, the fibres act as strain concentrators when the composite is loaded in the transverse direction with respect to the reinforcing fibres. From the bulk polymer measurements it is known that the PLLA cannot bear high strains prior to failure. Thus, the PLLA composites fail at rather low stresses because of the high strains that occur locally around the fibres. The EP exhibited a similar brittle material behaviour. However, the EP matrix NF-composite properties are not discussed here since the adhesion between the flax fibres and EP is not purely a physical interaction but includes covalent bonding. In contrast, the coPOM and coPOM_GV10 matrix NF-composites are able to resist higher strains because of the polymer's ability to deform plastically as shown in the bulk properties resulting in their relative higher transverse mechanical properties.

5. Conclusions

The modulus and the strength of fibre-reinforced composites, in particular natural fibre thermoplastic composites, depend strongly on the polymer bulk properties, the fibre impregnation and the properties of the fibre/matrix interface. In this study, the flexural modulus and strength in longitudinal and transverse fibre direction were measured and correlated to the interfacial properties. It was found that the strength in both longitudinal and transverse direction correlates well with the interface properties. The higher the work of adhesion (W_a) the higher the strength in longitudinal direction, suggesting a better stress transfer until the maximum load carrying ability is reached. In the transverse direction, the loading conditions are different and W_a relates more closely to the fibre/matrix interface. However, transverse properties are also affected by the impregnation of the technical fibres along with the bulk polymer mechanical behaviour. The W_a correlates also well with the composite's transversal strength for matrices that were able to deform plastically after reaching their yielding stress. In composites with brittle matrices such as PLLA, the high strains around the fibres cannot be sustained and the NF-composites fail at low strength. This means that the high W_a does not give entirely the full picture of the mechanical properties without also considering the impregnation and polymer yield behaviour.

By comparing theoretical and measured moduli, the EP matrix NF-composites showed the highest efficiency, closely followed by the PLLA matrix NF-composites. PLLA bulk polymers exhibited similar properties as EP, making it an interesting thermoplastic matrix material substitute. In addition, coPOM is an excellent polymer in NF composites, with high longitudinal properties and excellent transverse properties. With the coPOM, inherent thermoplastic short comings such as high creep can be addressed by locally tailoring, the properties using the coPOM_GV10. Similar to PLLA, the coPOM_GV10 polymer has properties as good as EP.

In this study, it is shown that thermoplastic polymers are suitable matrices for natural fibre-reinforced composites. By studying the bulk properties, applying appropriate processing conditions such as compression moulding in a closed mould, together with surface energy analysis to assess the spreading of the polymer on the fibre and the interface strength in the composite, one can design high-performance natural fibre-reinforced thermoplastic composites. The findings of this study will help to drive the applications of NFC towards structural components whilst demonstrating circularity and reduced ecological footprint and they have significant relevance in the emerging field of high-performance materials from renewable resources.

Acknowledgments

The authors would like to thank E. Kramer, V. Rumpf, A. Bian, L.Q.N Tran and C. Gosrani for their support with the experiments and helpful discussions. This research project was financially supported by the Innosuisse Swiss Innovation Agency 15091.1 PFIW-IW HIPETCONF and the Swiss Competence Center for Energy Research SCCER Mobility and the Gebert Rüf Stiftung, grant 077/15.

References

[1] Witik RA, Payet J, Michaud V, Ludwig C, Månson JAE. Assessing the life cycle costs and environmental performance of lightweight materials in automobile applications. Compos Part A Appl Sci Manuf 2011;42:1694–709. https://doi.org/10.1016/j.compositesa.2011.07.024.
[2] Oksman K, Skrifvars M, Selin J-F. Natural fibres as reinforcement in polylactic acid (PLA) composites. Compos Sci Technol 2003;63:1317–24. https://doi.org/10.1016/S0266-3538(03)00103-9.
[3] Joshi S, Drzal L, Mohanty A, Arora S. Are natural fiber composites environmentally superior to glass fiber reinforced composites? Compos Part A Appl Sci Manuf 2004;35:371–6. https://doi.org/10.1016/j.compositesa.2003.09.016.
[4] Shah DU, Porter D, Vollrath F. Can silk become an effective reinforcing fibre? A property comparison with flax and glass reinforced composites. Compos Sci Technol 2014;101:173–83. https://doi.org/10.1016/j.compscitech.2014.07.015.
[5] Barth M, Carus M. Multi hemp carbon footprint and sustainability of different natural fibres for biocomposites and insulation material; 2015.
[6] Song YS, Youn JR, Gutowski TG. Life cycle energy analysis of fiber-reinforced composites. Compos Part A Appl Sci Manuf 2009;40:1257–65. https://doi.org/10.1016/j.compositesa.2009.05.020.
[7] Wambua P, Ivens J, Verpoest I. Natural fibres: can they replace glass in fibre reinforced plastics? Compos Sci Technol 2003;63:1259–64. https://doi.org/10.1016/S0266-3538(03)00096-4.
[8] Dicker MPM, Duckworth PF, Baker AB, Francois G, Hazzard MK, Weaver PM. Green composites: a review of material attributes and complementary applications. Compos Part A Appl Sci Manuf 2014;56:280–9. https://doi.org/10.1016/j.compositesa.2013.10.014.
[9] Duc F, Bourban PE, Plummer CJG, Månson JaE. Damping of thermoset and thermoplastic flax fibre composites. Compos Part A Appl Sci Manuf 2014;64:115–23. https://doi.org/10.1016/j.compositesa.2014.04.016.
[10] Baley C. Analysis of the flax fibres tensile behaviour and analysis of the tensile stiffness increase. Compos Part A Appl Sci Manuf 2002;33:939–48. https://doi.org/10.1016/S1359-835X(02)00040-4.
[11] Rueppel M, Rion J, Dransfeld C, Fischer C, Masania K. Damping of carbon fibre and flax fibre angle-ply composite laminates. Compos Sci Technol 2017;146:1–9. https://doi.org/10.1016/j.compscitech.2017.04.011.
[12] Masania K, Woigk W, Rion J, Dransfeld C, Materials C. Effect of fibre volume content on the mechanical performance of natural fibre reinforced thermoplastic. In: ECCM 2016 - Proceeding 17th Eur. Conf. Compos. Mater., vol. C; 2016. p. 26–30.
[13] Bos HL, Van Den Oever MJA, Peters OCJJ. Tensile and compressive properties of flax fibres for natural fibre reinforced composites. J Mater Sci 2002;37:1683–92. https://doi.org/10.1023/A:1014925621252.
[14] Frey M, Biffi G, Adobes-Vidal M, Zirkelbach M, Wang Y, Tu K, et al. Tunable Wood by Reversible Interlocking and Bioinspired Mechanical Gradients. Adv Sci 2019. https://doi.org/10.1002/advs.201802190.
[15] Doan TTL, Brodowsky H, Mäder E. Jute fibre/epoxy composites: Surface properties and interfacial adhesion. Compos Sci Technol 2012;72:1160–6. https://doi.org/10.1016/j.compscitech.2012.03.025.
[16] Fuentes CA, Tran LQN, Van Hellemont M, Janssens V, Dupont-Gillain C, Van Vuure AW, et al. Effect of physical adhesion on mechanical behaviour of bamboo fibre reinforced thermoplastic composites. Colloids Surf A Physicochem Eng Asp 2013;418:7–15. https://doi.org/10.1016/j.colsurfa.2012.11.018.
[17] Pucci MF, Liotier PJ, Seveno D, Fuentes C, Van Vuure A, Drapier S. Wetting and swelling property modifications of elementary flax fibres and their effects on the Liquid Composite Molding process. Compos Part A Appl Sci Manuf 2017;97:31–40. https://doi.org/10.1016/j.compositesa.2017.02.028.
[18] Fuentes CA, Zhang Y, Guo H, Woigk W, Masania K, Dransfeld C, et al. Predicting the adhesion strength of thermoplastic/glass interfaces from wetting measurements. Colloids Surf A Physicochem Eng Asp 2018;558:280–90. https://doi.org/10.1016/j.colsurfa.2018.08.052.

[19] Van de Velde K, Kiekens P. Effect of material and process parameters on the mechanical properties of unidirectional and multidirectional flax/polypropylene composites. Compos Struct 2003;62:443–8. https://doi.org/10.1016/j.compstruct.2003.09.018.
[20] Holbery J, Houston D. Natural-fibre-reinforced polymer composites in automotive applications. J Miner Met Mater Soc 2006;58:80–6. https://doi.org/10.1007/s11837-006-0234-2.
[21] Bodros E, Pillin I, Montrelay N, Baley C. Could biopolymers reinforced by randomly scattered flax fibre be used in structural applications? Compos Sci Technol 2007;67:462–70. https://doi.org/10.1016/j.compscitech.2006.08.024.
[22] Fuentes CA, Willekens P, Petit J, Thouminot C, Müssig J, Trindade LM, et al. Effect of the middle lamella biochemical composition on the non-linear behaviour of technical fibres of hemp under tensile loading using strain mapping. Compos Part A Appl Sci Manuf 2017;101:529–42. https://doi.org/10.1016/j.compositesa.2017.07.017.
[23] Romhány G, Karger-Kocsis J, Czigány T. Tensile fracture and failure behavior of technical flax fibers. J Appl Polym Sci 2003;90:3638–45. https://doi.org/10.1002/app.13110.
[24] Perremans D, Hendrickx K, Verpoest I, Van Vuure AW. Effect of chemical treatments on the mechanical properties of technical flax fibres with emphasis on stiffness improvement. Compos Sci Technol 2018;160:216–23. https://doi.org/10.1016/j.compscitech.2018.03.030.
[25] Charlet K, Jernot JP, Eve S, Gomina M, Bréard J. Multi-scale morphological characterisation of flax: from the stem to the fibrils. Carbohydr Polym 2010;82:54–61. https://doi.org/10.1016/j.carbpol.2010.04.022.
[26] Barthelat F, Yin Z, Buehler MJ. Structure and mechanics of interfaces in biological materials. Nat Rev Mater 2016;16007. https://doi.org/10.1038/natrevmats.2016.7.
[27] Shah DU. Natural fibre composites: comprehensive Ashby-type materials selection charts. J Mater 2014;62:21–31. https://doi.org/10.1016/j.matdes.2014.05.002.
[28] Wielage B, Lampke T, Marx G, Nestler K, Starke D. Thermogravimetric and differential scanning calorimetric analysis of natural fibres and polypropylene. Thermochim Acta 1999;337:169–77. https://doi.org/10.1016/S0040-6031(99)00161-6.
[29] Faruk O, Bledzki AK, Fink H-P, Sain M. Biocomposites reinforced with natural fibers: 2000–2010. Prog Polym Sci 2012;37:1552–96. https://doi.org/10.1016/j.progpolymsci.2012.04.003.
[30] Tabone MD, Cregg JJ, Beckman EJ, Landis AE. Sustainability metrics: Life cycle assessment and green design in polymers. Environ Sci Technol 2010;44:8264–9. https://doi.org/10.1021/es101640n.
[31] Sabic. Technical Data Sheet - PP 515A; 2014.
[32] Sulzer. Technical Data Sheet - Sulzer Polylactides (PLA); 2012.
[33] Ticona. Technical Data Sheet - HOSTAFORM C 9021 GV1/10 - POM-GF10; 2011.
[34] Ticona. Technical Data Sheet - HOSTAFORM ® C 9021 XAP ® | POM | Unfilled; 2008.
[35] Fuentes CA, Tran LQN, Dupont-Gillain C, Vanderlinden W, De Feyter S, Van Vuure AW, et al. Wetting behaviour and surface properties of technical bamboo fibres. Colloids Surf A Physicochem Eng Asp 2011;380:89–99. https://doi.org/10.1016/j.colsurfa.2011.02.032.
[36] Andrieu C, Sykes C, Brochard F. Average spreading parameter on heterogeneous surfaces. Langmuir 1994;10:2077–80. https://doi.org/10.1021/la00019a010.
[37] Della Volpe C, Maniglio D, Siboni S, Morra M. Recent theoretical and experimental advancements in the application of van Oss–Chaudury–Good acid–base theory to the analysis of polymer surfaces I. General aspects. J Adhes Sci Technol 2003;17:1477–505. https://doi.org/10.1163/156856103769207365.
[38] Della Volpe C, Brugnara M, Maniglio D, Siboni S, Wangdu T. About the possibility of experimentally measuring an equilibrium contact angle and its theoretical and practical consequences. Contact Angle. Wettability Adhes 2006;4:79–99.
[39] Keller A, Dransfeld C, Masania K. Flow and heat transfer during compression resin transfer moulding of highly reactive epoxies. Compos Part B Eng 2018;153:167–75. https://doi.org/10.1016/j.compositesb.2018.07.041.
[40] Bachmann B, Masania K, Dransfeld C. The compression resin transfer moulding process for efficient composite manufacture. In: Proc 19th Int Conf Compos Mater - ICCM19; 2013. p. 8931–41.
[41] Defoirdt N, Biswas S, De Vriese L, Tran LQN, Van Acker J, Ahsan Q, et al. Assessment of the tensile properties of coir, bamboo and jute fibre. Compos Part A Appl Sci Manuf 2010;41:588–95. https://doi.org/10.1016/j.compositesa.2010.01.005.
[42] Tomczak F, Sydenstricker THD, Satyanarayana KG. Studies on lignocellulosic fibers of Brazil. Part II: Morphology and properties of Brazilian coconut fibers. Compos Part A Appl Sci Manuf 2007;38:1710–21. https://doi.org/10.1016/j.compositesa.2007.02.004.
[43] Mezger TG. The rheology handbook: for users of rotational and oscillatory rheometers. Vincentz Network; 2011.
[44] Darcy H. Les fontaines publiques de la ville de Dijon: exposition et application... Victor Dalmont; 1856.
[45] Fratzl P, Weinkamer R. Nature's hierarchical materials. Prog Mater Sci 2007;52:1263–334. https://doi.org/10.1016/j.pmatsci.2007.06.001.
[46] Aranberri-Askargorta I, Lampke T, Bismarck A. Wetting behavior of flax fibers as reinforcement for polypropylene. J Colloid Interface Sci 2003;263:580–9. https://doi.org/10.1016/S0021-9797(03)00294-7.
[47] Shen Q, Mikkola P, Rosenholm JB. Quantitative characterization of the subsurface acid-base properties of wood by XPS and Fowkes theory. Colloids Surf A Physicochem Eng Asp 1998;145:235–41. https://doi.org/10.1016/S0927-7757(98)00655-4.
[48] Johansson LS, Campbell JM, Koljonen K, Stenius P. Evaluation of surface lignin on cellulose fibers with XPS. Appl Surf Sci 1999;144–145:92–5. https://doi.org/10.1016/S0169-4332(98)00920-9.
[49] Tran LQN, Fuentes CA, Dupont-Gillain C, Van Vuure AW, Verpoest I. Wetting analysis and surface characterisation of coir fibres used as reinforcement for composites. Colloids Surfaces A Physicochem Eng Asp 2011;377:251–60. https://doi.org/10.1016/j.colsurfa.2011.01.023.
[50] Fuentes CA, Brughmans G, Tran LQN, Dupont-Gillain C, Verpoest I, Van Vuure AW. Mechanical behaviour and practical adhesion at a bamboo composite interface: Physical adhesion and mechanical interlocking. Compos Sci Technol 2015;109:40–7. https://doi.org/10.1016/j.compscitech.2015.01.013.
[51] Fowkes FM. Quantitative characterization of the acid-base properties of solvents, polymers, and inorganic surfaces. J Adhes Sci Technol 1990;4:669–91. https://doi.org/10.1163/156856190X00595.
[52] Lavielle L, Schultz J, Nakajima K. Acid–base surface properties of modified poly (ethylene terephthalate) films and gelatin: relationship to adhesion. J Appl Polym Sci 1991;42:2825–31. https://doi.org/10.1002/app.1991.070421021.
[53] Shah DU, Schubel PJ, Clifford MJ, Licence P. The tensile behavior of off-axis loaded plant fiber composites: an insight on the nonlinear stress–strain response. Polym Compos 2012;33:1494–504. https://doi.org/10.1002/pc.22279.
[54] Baley C, Perrot Y, Busnel F, Guezenoc H, Davies P. Transverse tensile behaviour of unidirectional plies reinforced with flax fibres. Mater Lett 2006;60:2984–7. https://doi.org/10.1016/j.matlet.2006.02.028.
[55] Luo S, Netravali AN. Mechanical and thermal properties of environment-friendly "green" composites made from pineapple leaf fibers and poly(hydroxybutyrate-co-valerate) resin. Polym Compos 1999;20:367–78. https://doi.org/10.1002/pc.10363.